NANO LETTERS

2004
Vol. 4, No. 11
2227−2232

Synthesis of Silver Nanoparticles in a Continuous Flow Tubular Microreactor

Xue Zhang Lin, Alexander D. Terepka, and Hong Yang*

Department of Chemical Engineering, 206 Gavett Hall, University of Rochester, Rochester, New York 14627-0166

Received August 31, 2004; Revised Manuscript Received September 30, 2004

ABSTRACT

This paper describes the synthesis of silver nanoparticles in a continuous flow tubular microreactor using silver pentafluoropropionate as a single-phase reactant precursor. This precursor can be thermally reduced in isoamyl ether to form silver nanoparticles in the presence of trioctylamine. The reaction is suitable for continuous flow reactors because of the moderate temperature for the formation of silver nanoparticles. The produced silver nanoparticles can have a narrow size distribution. Temperature profiles of the reactant fluids are obtained to understand the formation of silver nanoparticles in the microreactor.

Scaled-up production of monodisperse colloidal nanoparticles has become an important research subject in recent years. In this regard, continuous flow reactors are generally favored over batch reactors. Decomposition of organometallic precursors in organic solvents is one of the most commonly used approaches to nanoparticles because the narrow size distribution can be achieved in such reaction systems.[1,2] Rapid injection of precursors into a heated mixture of solvent, coordinating ligands, and other precursors is often required. A batch process is suitable for those reactions, but often limited to small-scale synthesis due to the low production yield of nanoparticles and the time-consuming nature of the process. A flow reactor, on the other hand, can generate products on a continuous basis once the reaction reaches steady state and is more appropriate for a large-scale production than the batch reactor. Furthermore, targeted reaction temperatures can be achieved in second or even millisecond time scales in a microreactor.

Microfluidic reactors have recently been used in the synthesis of various organic, inorganic, and biological materials.[3−9] For the synthesis of colloidal nanoparticles, attention has largely focused on various semiconducting materials. Several groups have recently used fluidic microreactors[10−14] to make semiconductor nanoparticles of CdSe[10−13] and TiO_2,[14] although the size distribution of these nanoparticles varies substantially depending on the procedure used. These continuous flow processes usually require well-mixed solutions in order to form narrowly dispersed nanoparticles if several reactants are involved. Mixing is largely mediated by molecular diffusion and can be slow. As a result, micromixers are often used in the synthesis of semiconductor nanoparticles, because two or multiphase reactants are involved.[10] In addition to semiconductor nanoparticles, Wagner et al. recently used preformed citrate-stabilized gold nanoparticles as seeds to grow large nanoparticles in a microreactor. The gold particles formed were polydisperse using this process.[15] These experiments, nevertheless, demonstrate the potential of using fluidic microreactors for making nanoparticles in a continuous process. To the best of our knowledge, no direct synthesis of metallic silver nanoparticles in a microreactor based on a single-phase precursor has been reported. A single-phase reactant system can be very useful, because it can eliminate the need for a mixer.

In this paper, we demonstrate the synthesis of monodisperse silver nanoparticles using thermal reduction of silver pentafluoropropionate in isoamyl ether in a continuous flow tubular microreactor. We have previously used this approach for making narrowly dispersed silver nanoparticles from silver trifluoroacetate,[16] since silver carboxylates are precursors that can be thermally reduced under moderate conditions.[17−19] Unlike the commonly used methods for making silver nanoparticles from silver salts in aqueous solutions, the thermal reducible mixture used in this work is a single-phase system, which is suitable for generating narrowly dispersed nanoparticles without the size-selection procedure. Silver pentafluoropropionate was chosen as precursor and trioctylamine (TOA) as surfactant because of their good solubility in isoamyl ether. Silver nanoparticles can also form rapidly, typically within minutes, in microreactors.

In a typical procedure, silver pentafluoropropionate (98%, Aldrich, 0.08 g) and trioctylamine (98%, Aldrich, 386 μL) were dissolved in isoamyl ether (99%, Aldrich, 6 mL). The molar ratio between the silver precursor and surfactant was 1:3 unless otherwise indicated. This solution was introduced

* Corresponding author. E-mail: hongyang@che.rochester.edu.

10.1021/nl0485859 CCC: $27.50
Published on Web 10/14/2004

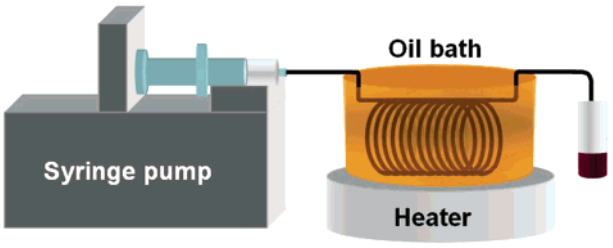

Figure 1. Experimental setup of the synthesis of Ag nanoparticles in a tubular microreactor.

into a tubular coil made of stainless steel needle (gauge no. 18, i.d. 0.84 mm, Popper & Sons, Inc.) using a syringe (Norm-Ject 2 mL, Henke-Sass Wolf). Figure 1 is an illustration of the experimental setup. A syringe pump (model: Harvard Apparatus 55-4140) was used to regulate the flow rates which were between 0.08 and 0.7 mL min^{-1}. The length of the stainless steel tube immersed in the oil bath was ~20±0.5 cm. Both the diameter of the helical coil and the pitch length were ~2 cm. This tubular microreactor was heated to a designed temperature between 100 and 140 °C using an oil bath with a stirrer/hot plate (Chemglass analog hotplate stirrer). The product was collected in a glass vial, and oleylamine (70%, Aldrich, 40 μL) was added subsequently to stabilize Ag nanoparticles for long-term storage. After the reaction, the stainless steel tube was cleaned with an aqueous solution (30 mL) of potassium ferricyanide (III) (0.098 g), potassium hexacyanoferrate (II) trihydrate (0.012 g), and potassium thiosulfate hydrate (0.65 g), and further rinsed with hexane.

Transmission electron microscopy (TEM) images were recorded on a JEOL JEM 2000EX microscope at an accelerating voltage of 200 kV. In the preparation of specimen, Ag nanoparticles were precipitated by adding ethanol to the suspension at an ethanol/mixture volume ratio of 6.5:1 and then separated from the supernatant by centrifuging at 5000 rpm for 5 min under ambient conditions. The particles obtained were dispersed in hexane, and finally a drop of this silver nanoparticle suspension was drop-cast on a carbon-coated copper grid. The ultraviolet−visible (UV−vis) spectra of Ag nanoparticles were recorded using a Perkin-Elmer Lambda 900 UV/VIS/NIR spectrometer. The sample was prepared by diluting 20 μL of as-synthesized mixture with 3 mL of hexane. The particle size distribution was analyzed by measuring between 250 and 400 nanoparticles based on TEM micrographs using Scion Image Software 4.0.2 (Scion Corp).

Both silver pentafluoropropionate and TOA were soluble in isoamyl ether, resulting in a colorless transparent solution. This solution was introduced by the syringe pump into the tubular microreactor immersed in the oil bath at a designed temperature. The color of the reaction mixture turned into dark brown, which indicated the formation of silver nanoparticles. Oleylamine was the capping agent used to stabilize Ag nanoparticles[20] and was added into the product solutions for long-term storage. Silver nanoparticles were separated from solvent mixture using ethanol as antisolvent.

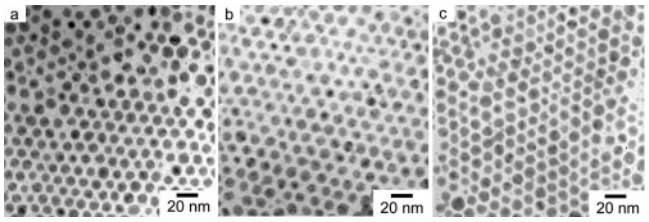

Figure 2. TEM images of Ag nanoparticles made at the trioctylamine/silver pentafluoropropionate molar ratios of (a) 3:1, (b) 6:1, and (c) 12:1. The reaction temperature was 100 °C and the flow rate was 0.08 mL min^{-1}.

Table 1. Particle Size Analysis of Ag Nanoparticles Synthesized at the Different Molar Ratios and Reaction Temperatures

sample no.	molar ratio of TOA/silver pentafluoropropionate	reaction temp (° C)	particle size (nm) average diameter	particle size (nm) standard deviation
2a	3	100	8.7	0.9
2b	6	100	8.6	0.9
2c	12	100	8.6	1.0
6a	3	120	8.3	1.2
6b	3	140	7.4	1.4

Figure 2 shows the TEM images of silver nanoparticles made at TOA/silver pentafluoropropionate molar ratios of 3, 6, and 12, respectively. The flow rate in these cases was set at 0.08 mL min^{-1} and the temperature of oil bath was set at 100 °C. The silver nanoparticles were rather narrowly dispersed in size and had an average diameter of 8.7 ± 0.9 nm at a surfactant/silver precursor ratio of 3. TEM study shows that average diameters were 8.6 ± 0.9 and 8.6 ± 1.0 nm for the molar ratios of TOA/silver pentafluoropropionate of 6 and 12, respectively. The size and the size distribution of Ag nanoparticles are summarized in Table 1. These results indicated that the change in TOA concentration did not lead to a substantial difference in either the size or size distribution of the nanoparticles. Greenish residue suspension could form in the tube after the reaction, as a small amount of large aggregates was found after the tube was drained. Such aggregates did not show up in the production and could be due to the accumulation of silver nanoparticles on the inner surface of the stainless steel wall. One possible reason could be that the bulky TOA could not stabilize the Ag particles. The aggregation of nanoparticles could be avoided by addition of ~30 μL of oleylamine in the feed solution together with TOA and silver pentafluoropropionate. The size of the particles produced, however, became less monodisperse than that without oleylamine. Thus, we chose to add oleylamine in the product solution to stabilize the Ag nanoparticles.

The flow rate, flow pattern, and reactor temperature could significantly affect the size and size distribution of Ag nanoparticles. As the flow rates increased from 0.08 to 0.6 mL min^{-1}, UV−vis absorbance peaks of produced Ag nanoparticles broadened, as shown in Figure 3. The values of full width at half-maximum (FWHM) for samples at the various flow rates are summarized in the table presented in Figure 3. The observed broadening in absorbance suggests

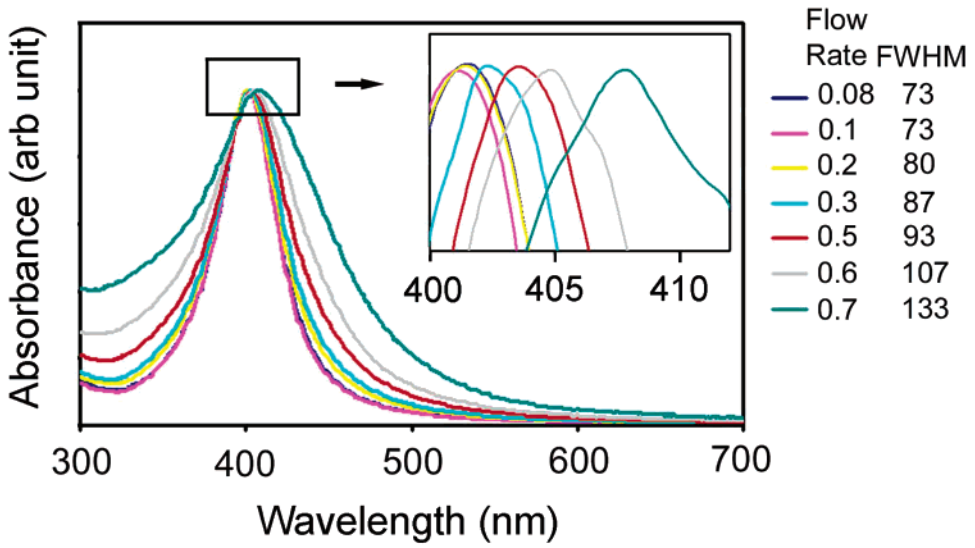

Figure 3. (a) UV−vis absorption spectra of silver nanoparticles made at the different flow rates. Insets show the enlarged peak region (400−412 nm) and a summary of FWHMs of the absorbance of the Ag nanoparticles (in nm) at the various volumetric flow rates (in mL min^{-1}) used.

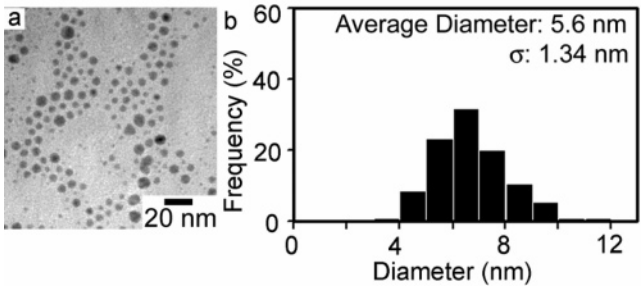

Figure 4. TEM image and the corresponding particle size distribution analysis of the Ag nanoparticles made in the tubular microreactor at a flow rate of 0.6 mL min^{-1}.

Table 2. Volumetric and Linear Flow Rates, Reynolds Numbers, Resident Times, and Effective Resident Times of the Fluids in the Flow Tubular Microreactor

flow rate (mL min^{-1})	u (m s^{-1})	Re	τ (s)	τ_{eff} (s)
0.08	0.0024	4.1	83	79
0.10	0.0030	5.1	67	63
0.20	0.0060	10	33	30
0.30	0.0090	15	22	19
0.50	0.015	26	13	10
0.60	0.018	31	11	8
0.70	0.021	36	10	6

that the nanoparticles became polydisperse[21,22] at the high flow rates. At the flow rate of 0.08 mL min^{-1}, the average diameter of the Ag nanoparticles was 8.7 ± 0.9 nm and the FWHM in UV−vis absorbance was 73 nm. As the flow rate increased to 0.6 mL min^{-1}, the particle formed became polydisperse and the diameters of the nanoparticles varied between 3 and 12 nm, Figure 4. The average diameter of nanoparticles was also reduced to 5.6±1.3 nm with a standard deviation of ∼20%. For this sample, the FWHM in UV−vis absorbance was about 107 nm.

To determine the flow patterns, Reynolds numbers, Re, of the fluids were calculated using the following equation:[23]

$$\mathrm{Re} = \frac{uD}{\nu} \qquad (1)$$

where u is the linear flow velocity, D is the inert diameter of the tube, and ν is kinematic viscosity of the fluid, which can be obtained using dynamic viscosity divided by the density of the fluid. In this study, we assumed the solutes did not drastically change the viscosity of the fluid and the values for isoamyl ether were used. Table 2 shows the values of Re at the various flow rates and at the temperature of 100 °C. In all cases, Re numbers were far below the critical value of 2100, indicating the flows were laminar. Such flows took on a parabolic velocity profile and thus the nanoparticles formed in the center moved faster than those near the wall region. This nonuniformity in velocity profile could potentially cause the polydispersity of nanoparticles at a high flow rate in the microreactor.[10] The resident time of the fluids in the tube, τ, was another critical factor for the formation of Ag nanoparticles. These values at different flow rates were calculated based on the flow rates and the length of microtube immersed in the oil bath (∼20 cm), Table 2. For this reaction system, a resident time of ∼60 s was required in order to obtain narrowly dispersed silver nanoparticles when the reaction temperature was 100 °C. Resident times shorter than 60 s resulted in smaller average diameters and broader size distributions of nanoparticles, Figure 4.

Reaction temperature played a crucial role in the formation of Ag nanoparticles. When the temperature was below ∼100 °C, no silver particle formed after the reactants flowed through the tubular microreactor at the rate of 0.08 mL min^{-1}. It appeared that the silver pentafluoropropionate started to decompose and form Ag nanoparticles at the temperatures

of ~100 °C or above. Thus we examined the position in the tubular microreactor at which the fluid reached this temperature.

Temperature profiles were calculated for the two extreme flow rates used in order to find out the position and the time needed for the fluid to reach the steady-state condition inside the tube. These profiles were calculated for the fluid in the region of the reactor immersed in the oil bath. We made the following further assumptions in the calculation: the fluid had a fully developed laminar flow pattern in the microreactor with a constant wall temperature. Temperature gradient along the radius direction inside the tube was not taken into consideration. Forced convection heat transfer was used, since the fluid was pressed into the microreactor by a syringe pump. To obtain the temperature profiles in a helical tube, we calculated three dimensionless numbers including Prandtl number, Pr, helical number, He, and Nusselt number, Nu. Prandtl number was obtained using the following relation:[23]

$$\mathrm{Pr} = \frac{C_p \times \mu}{k} \tag{2}$$

where C_p is specific heat for isoamyl ether (2.40 kJ kg^{-1} °C^{-1});[24] μ is dynamic viscosity for isoamyl ether (1.07 × 10^{-3} kg s^{-1} m^{-1} at 290 K and 0.375 × 10^{-3} kg s^{-1} m^{-1} at 375 K);[25] and k is the thermal conductivity of the fluid. The value for k is estimated to be 0.12 W m^{-1} °C^{-1} using the value of pentyl ether, which has similar molecule weight, density, and boiling point as those for isoamyl ether (173 °C for isoamyl ether and 188 °C for pentyl ether).[26] The relation between helical number, He, and Reynolds number, Re, is given by:[27]

$$\mathrm{He} = \mathrm{Re}\left(\frac{r}{R_c}\right)^{1/2} \tag{3}$$

where r is the radius of the tube, and R_c is the critical radius of the helical coil that is determined by the radius of the helical R, and the pitch length of the helical coils, p, using the following equation:

$$R_c = R\left(1 + \frac{p}{2\pi R}\right) \tag{4}$$

The Nusselt number, Nu, was calculated based on the Manlapaz-Churchill correlation:[27]

$$\mathrm{Nu} = \left[\left(3.657 + \frac{4.343}{\left(1 + \frac{957}{\mathrm{Pr} \times \mathrm{He}^2}\right)^2}\right)^3 + 1.158 \times \left(\frac{\mathrm{He}}{1 + \frac{0.477}{\mathrm{Pr}}}\right)^{3/2}\right]^{1/3} \tag{5}$$

From the Nusselt number, Nu, we could obtain the heat transfer coefficient, h, using the equation[23]

$$h = \frac{k \times \mathrm{Nu}}{D} \tag{6}$$

and temperature, T_L, at a given position along the tube length, L, based on energy balance using the following expression:

$$\frac{T_L - T_o}{T_w - T_L} = \frac{\pi \times D \times h \times L}{m \times C_p} \tag{7}$$

where T_o is the temperature of the fluid at the inlet of the reactor (20 °C); T_w is the wall temperatures of the microreactor (100−140 °C); and m is the mass flow rate of the fluid (1.04 × 10^{-6} kg s^{-1} at volumetric flow rate of 0.08 mL min^{-1}). The density of isoamyl ether of 778 kg m^{-3} was used in the calculation.[24]

Figure 5 shows the calculated temperature profiles for fluids in the helical tube at the flow rates of 0.08 and 0.6 mL min^{-1}, respectively. The wall temperature was 100 °C. Heat flux decreased rapidly in the direction of flow, leading to a progressively reduced rate of temperature change in the fluid along the tube direction. At the flow rate of 0.08 mL min^{-1}, the solution reached 100 °C in ~4 s and within the first centimeter after it entered the heating zone of the tube. Since silver pentafluoropropionate thermally decomposed at this temperature, the effective resident time, τ_{eff}, which was estimated based on the length of the tube when fluid reached the reaction temperature of 100 °C, was about 79 s, Table 2. This reaction time appeared to be sufficient for the formation and growth of nanoparticles. When flow rates increased, longer distances were required for the reaction fluid to reach this reaction temperature. For example, the fluid reached 100 °C at a point of ~6 cm after entering the heating zone when the flow rate was 0.6 mL min^{-1}. This result implies that the reaction started ~6 cm away from the point where tube immersed in the oil bath. The reaction occurred within the remaining portion of the microtube (14 cm); thus the effective resident time was much shorter than that at a low flow rate. The effective resident time in this case was only ~8 s, Table 2. As a result, silver pentafluoropropionate might not have sufficient time to react completely at this flow rate before it exited the tubular reactor. The product at a flow rate > 0.6 mL min^{-1} was typically light brown, indicating a low concentration of Ag nanoparticles. We were able to make narrowly dispersed Ag nanoparticles at a volumetric flow rate of 0.1 mL min^{-1} as well. Nanoparticles made at this flow rate had a similar FWHM in UV−vis absorbance as those formed at a volumetric flow rate of 0.08 mL min^{-1}, Figure 3. The values of FWHM increased rapidly when the flow rates were equal to or greater than 0.2 mL min^{-1}, suggesting that the Ag nanoparticles formed became polydisperse. We concluded that resident times of ~60 s or longer were required for the formation of narrowly dispersed nanoparticles of silver in this tubular microreactor at 100 °C.

We further examined the effect of reaction temperature on the size and size distribution of Ag nanoparticles. When the reaction temperature was set at 120 °C, the nanoparticles made became small and had an average diameter of 8.3 ±

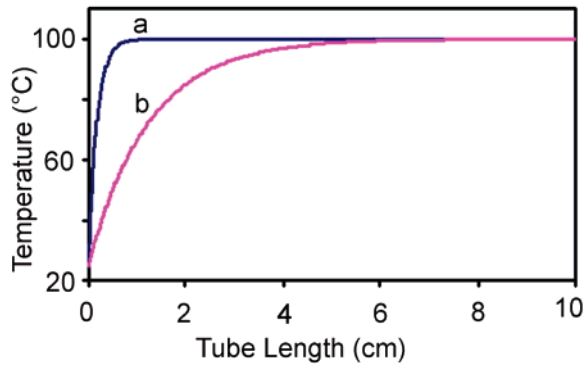

Figure 5. Calculated temperature profiles of the reaction fluids in the tubular microreactor along the direction of tube length at the flow rates of (a) 0.08 and (b) 0.6 mL min^{-1}.

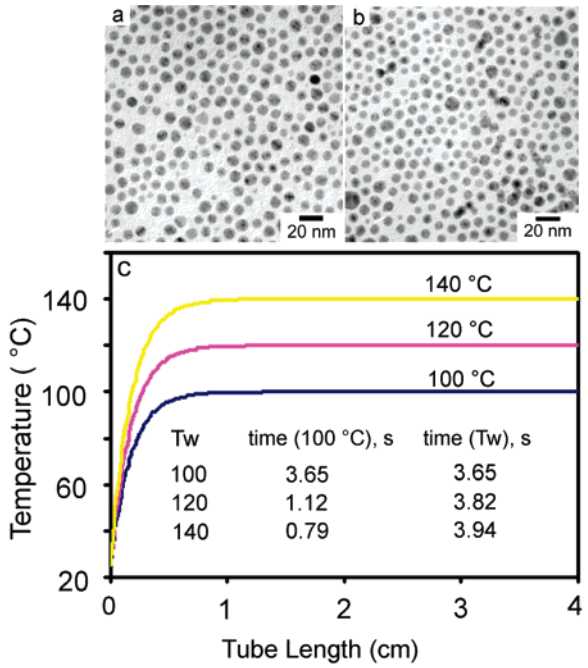

Figure 6. (a, b) TEM images of Ag nanoparticles formed at the wall temperatures of (a) 120 °C and (b) 140 °C, respectively, and (c) calculated temperature profiles of the fluid along the tube length with the wall temperatures, T_w, of 100, 120, and 140 °C, respectively. The table of the inset lists the time required for the fluid to reach the reaction (~100 °C) and wall temperatures, T_w.

1.2 nm, Figure 6a. Further increase in the reaction temperature to 140 °C led to the formation of even smaller nanoparticles with the average diameter of 7.4 ± 1.4 nm, Figure 6b. The size and the size distribution of these nanoparticles are summarized in Table 1. The size distributions of the particles formed at the high temperature were relatively broadened. When TOA was used as surfactant, temperature equal to or higher than 140 °C was not desirable for getting monodisperse nanoparticles. The possible reason could be due to the steric effect of the surfactant. The bulkiness of alkyl chain might prevent TOA from forming densely packed layers on the nanoparticle surfaces that were required for the stabilization of nanoparticles.

The temperature profiles of reaction mixtures were calculated for different wall temperatures in order to understand the temperature effects on the formation of nanoparticles, Figure 6c. The calculation was based on the Manlapaz-Churchill correlation of eq 5, and energy balance of eq 7. The results show that it took 3.65, 1.12, and 0.79 s for the fluid to reach the reaction temperature of about 100 °C, when the wall temperatures were at 100, 120, and 140 °C, respectively. The effective resident times were sufficient for the formation of narrowly dispersed Ag nanoparticles in these cases. This result suggests that the nuclei of the Ag nanoparticles formed continue to grow into large nanoparticles in the tubular microreactor, while TOA cannot effectively stabilize the nanoparticles particularly at these relatively high temperatures, resulting in the formation of polydisperse Ag nanoparticles.

In summary, we demonstrated that silver nanoparticles can be synthesized by using a continuous flow tubular reactor using silver pentafluoropropionate as single-phase precursor. The temperature profiles based on forced convection in a helical tubular microreactor can be used in understanding the formation of nanoparticles at various temperatures, flow rates, and reaction times. We believe that single-source precursors can have advantages in making monodisperse nanoparticles of silver and other materials using a continuous process. A continuous flow microreactor using a single-phase reaction system can be very valuable for the scale-up production of monodisperse nanoparticles.

Acknowledgment. This work was supported in part by NSF and NIEHS Environmental Health Sciences Center at University of Rochester. A.D.T. was a Pittsford Career Intern student. We thank Professor Matthew Yates to lend us the UV/VIS/NIR spectrometer.

References

(1) Murray, C. B.; Kagan, C. R.; Bawendi, M. G. *Annu. Rev. Mater. Sci.* **2000**, *30*, 545−610.
(2) Kreibig, U.; Bonnemann, H.; Hormes, J. In *Handbook of Surfaces and Interfaces of Materials: Nanostructured Materials, Micelles and Colloids*; Nalwa, H. S., Ed.; Academic Press: San Diego, 2001; Vol. 3, pp 1−85.
(3) Jahnisch, K.; Hessel, V.; Lowe, H.; Baerns, M. *Angew. Chem., Int. Ed.* **2004**, *43*, 406−446.
(4) Seong, G. H.; Crooks, R. M. *J. Am. Chem. Soc.* **2002**, *124*, 13360−13361.
(5) Kobayashi, J.; Mori, Y.; Okamoto, K.; Akiyama, R.; Ueno, M.; Kitamori, T.; Kobayashi, S. *Science* **2004**, *304*, 1305−1308.
(6) Wang, J.; Ibanez, A.; Chatrathi, M. P. *J. Am. Chem. Soc.* **2003**, *125*, 8444−8445.
(7) Arana, L. R.; Schaevitz, S. B.; Franz, A. J.; Schmidt, M. A.; Jensen, K. F. *J. Microelectromech. Syst.* **2003**, *12*, 600−612.
(8) Takayama, S.; Ostuni, E.; LeDuc, P.; Naruse, K.; Ingber, D. E.; Whitesides, G. M. *Nature* **2001**, *411*, 1016−1016.
(9) Zanzotto, A.; Szita, N.; Boccazzi, P.; Lessard, P.; Sinskey, A. J.; Jensen, K. F. *Biotechnol. Bioeng.* **2004**, *87*, 243−254.
(10) Yen, B. K. H.; Stott, N. E.; Jensen, K. F.; Bawendi, M. G. *Adv. Mater.* **2003**, *15*, 1858−1862.
(11) Chan, E. M.; Mathies, R. A.; Alivisatos, A. P. *Nano Lett.* **2003**, *3*, 199−201.
(12) Nakamura, H.; Yamaguchi, Y.; Miyazaki, M.; Maeda, H.; Uehara, M.; Mulvaney, P. *Chem. Commun.* **2002**, 2844−2845.
(13) Shestopalov, I.; Tice, J. D.; Ismagilov, R. F. *Lab Chip* **2004**, *4*, 316−321.
(14) Wang, H. Z.; Nakamura, H.; Uehara, M.; Miyazaki, M.; Maeda, H. *Chem. Commun.* **2002**, 1462−1463.
(15) Wagner, J.; Kirner, T.; Mayer, G.; Albert, J.; Kohler, J. M. *Chem. Eng. J.* **2004**, *101*, 251−260.
(16) Lin, X. Z.; Teng, X. W.; Yang, H. *Langmuir* **2003**, *19*, 10081−10085.

(17) Cowdery-Corvan, P. J.; Whitcomb, D. R. In *Handbook of Imaging Materials*, 2nd ed.; Diamond, A. S., Weiss, D. S., Eds.; Marcel Dekker: New York, 2002; pp 473−529.
(18) Fields, E. K.; Meyerson, S. *J. Org. Chem.* **1976**, *41*, 916−920.
(19) Lee, S. J.; Han, S. W.; Choi, H. J.; Kim, K. *J. Phys. Chem. B* **2002**, *106*, 2892−2900.
(20) Hiramatsu, H.; Osterloh, F. E. *Chem. Mater.* **2004**, *16*, 2509−2511.
(21) Pesika, N. S.; Stebe, K. J.; Searson, P. C. *J. Phys. Chem. B* **2003**, *107*, 10412−10415.
(22) Pesika, N. S.; Stebe, K. J.; Searson, P. C. *Adv. Mater.* **2003**, *15*, 1289−1291.
(23) Holman, J. P. In *Heat Transfer*, 6th ed.; McGraw-Hill: New York, 1986.
(24) Lide, D. R. *Handbook of Organic Solvents*; CRC Press: Boca Raton, 1995.
(25) Viswanath, D. S.; Natarajan, G. *Data Book on the Viscosity of Liquids*; Hemisphere Publishing: New York, 1989.
(26) Yaws, C. L. In *Handbook of Transport Property Data*; Gulf Publishing Co.: Houston, 1995.
(27) Manlapaz, R. L.; Churchill, S. W. *Chem. Eng. Commun.* **1981**, *9*, 185−200.

NL0485859